Geophysical Journal International

Geophys. J. Int. (2018) **213,** 824–835
Advance Access publication 2018 January 22
GJI Seismology

doi: 10.1093/gji/ggy022

Constraints on the structure of the crust and lithosphere beneath the Azores Islands from teleseismic receiver functions

Kathrin Spieker,[1,2] Stéphane Rondenay,[2] Ricardo Ramalho,[3,4,5] Christine Thomas[6] and George Helffrich[7]

[1] *Institute for Geophysics and Geology, University of Leipzig, Talstr.* 35, *D*-04103 *Leipzig, Germany. E-mail: kathrin.spieker@gmail.com*
[2] *Department of Earth Science, University of Bergen, Allégaten* 41, 5007 *Bergen, Norway*
[3] *Instituto Dom Luiz, Faculdade de Ciências, Universidade de Lisboa,* 1749-016 *Lisboa, Portugal*
[4] *School of Earth Sciences, University of Bristol, Bristol BS*8 1*TH, UK*
[5] *Lamont-Doherty Earth Observatory, Columbia University, Palisades, NY* 10964, *USA*
[6] *University of Münster, Institute for Geophysics, D*-48149 *Münster, Germany*
[7] *Tokyo Institute of Technology, Earth-Life Science Institute, Tokyo* 152-8550, *Japan*

Accepted 2018 January 21. Received 2017 November 14; in original form 2017 May 16

SUMMARY

The Azores Archipelago is located near the Mid-Atlantic Ridge (MAR) and consists of nine islands, resting on both sides of the ridge. Various methods including seismic reflection, gravity and passive seismic imaging have previously been used to investigate the crustal thickness beneath the islands. They have yielded thickness estimates that range between roughly 10 and 30 km, but until now models of the more fine-scale crustal structure have been lacking. Pending questions include the thickness of the volcanic edifice beneath the islands and whether crustal intrusions or even underplating can be observed beneath any island. In this study, we use data from nine seismic stations located on the Azores Islands to investigate the crustal structure with teleseismic *P*-wave receiver functions. Our results indicate that the base of the volcanic edifice is located approximately 1 to 4 km depth beneath the different islands and that the crust–mantle boundary has an average depth of ∼17 km. There is strong evidence for magmatic underplating beneath the island of São Jorge, and indications that the underplating is also present beneath São Miguel and possibly Santa Maria. Additionally, the seismological lithosphere–asthenosphere boundary, defined as a seismic velocity drop in the uppermost mantle, seems to deepen with increasing distance from the MAR. It has a depth of ∼45 km beneath the islands close to the MAR, compared to depths >70 km beneath the more distal islands.

Key words: Composition and structure of the oceanic crust; Atlantic Ocean; Crustal imaging; Crustal structure.

1 INTRODUCTION

The Azores Archipelago consists of nine volcanic islands located on both sides of the Mid-Atlantic Ridge (MAR). The islands can be divided into the Western Group comprising Flores and Corvo; the Central Group comprising São Jorge, Faial, Pico, Graciosa and Terceira; and the Eastern Group comprising São Miguel and Santa Maria. Three tectonic plates segment the Azores island region and form a triple junction: the North American plate, the Eurasian plate and the Nubian plate (Fig. 1). Whilst the Western Group is located to the west of the MAR, the remaining islands straddle the diffuse plate boundary between the Eurasian and Nubian plates (Madeira & Ribeiro 1990; Luis *et al*. 1994; Marques *et al*. 2013).

The Azores Islands rest on a wide triangular-shaped bathymetric anomaly—the Azores Plateau—roughly outlined by the −2000 m isobath (Searle 1980; Lourenço *et al*. 1998; Gente *et al*. 2003). This area of elevated seafloor corresponds to a massive volcanic plateau, interpreted as the result of the interaction of a mantle plume with the MAR (e.g. Schilling 1975; Gente *et al*. 2003). The development of the plateau is inferred to have occurred mainly between 20 and 7 Ma, and was followed by significant post-volcanic tectonic rifting (Gente *et al*. 2003; Luis & Miranda 2008). Whilst being stretched along the MAR, the plateau has been split into a smaller western and larger eastern sector. The incipient Princess Alice Rift and the later, more developed Terceira ultra-slow spreading ridge cut across the eastern sector (Luis & Miranda 2008; Miranda *et al*. 2015). In the past, the Terceira Ridge migrated northwards and its movement might be related to the relative motion of the plates with regard to a mantle plume (e.g. Luis *et al*. 1994) or to small changes in the relative motion of the three plates (e.g. Adam *et al*. 2013). Low seismic

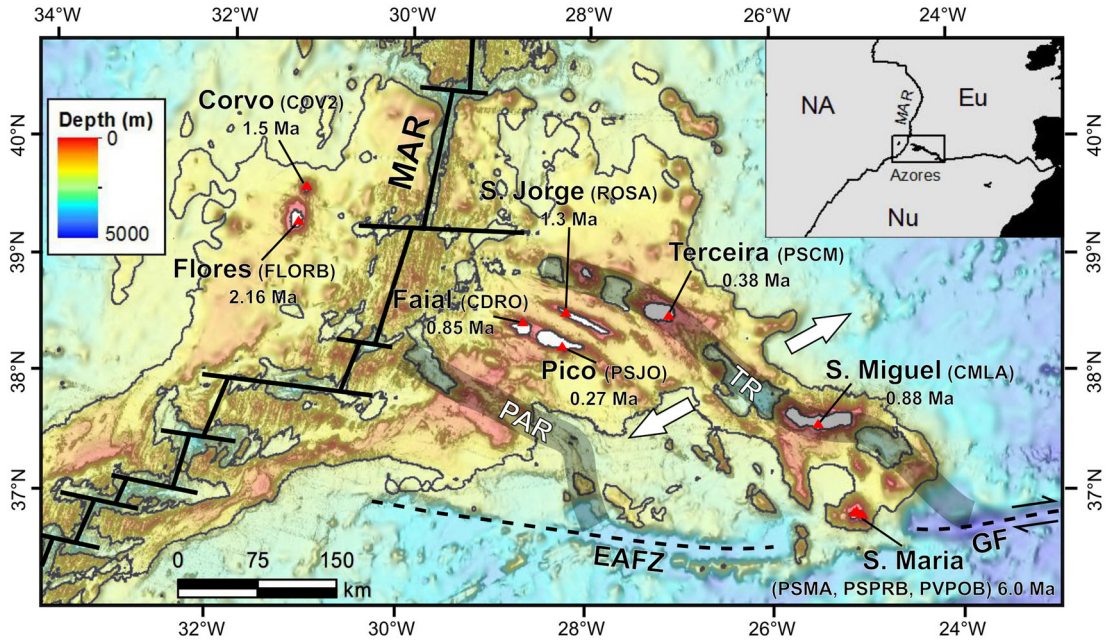

Figure 1. Setting of the Azores Islands with location of 10 seismic stations (names in brackets). The oldest radiometric age for each island are indicated (Chovelon 1982; Johnson *et al*. 1998; Azevedo & Ferreira 2006; Calvert *et al*. 2006; França *et al*. 2006; Hildenbrand *et al*. 2008; Hildenbrand *et al*. 2012; Sibrant *et al*. 2015a,b; Ramalho *et al*. 2017). TR, Terceira Ridge; MAR, Middle Atlantic Ridge; PAR, Princess Alice Ridge; EAFZ, East Azores Fracture Zone; GF, Glória Fault; Eu, Eurasian Plate; Nu, Nubian Plate; NA, North American Plate. Bathymetric data extracted from the EMODNET web portal (http://portal.emodnet-bathymetry.eu); −2000 m isobath shown in black.

velocity anomalies suggest that the plume may today be centred beneath the central island group (Schilling 1975; Ito & Lin 1995), with a possible second branch extending beneath the area surrounding Terceira and São Miguel (e.g. Silveira *et al*. 2006; Adam *et al*. 2013). The islands west of the MAR presumably were formed by a different process than the other islands, on account of different geochemical characteristics (Genske *et al*. 2016) and a different local tectonic setting. The youngest and most active islands are Faial, Terceira and Pico of the Central Group, and São Miguel located in the eastern part of the plateau. The easternmost island, Santa Maria, shows no sign of recent activity and hosts the oldest rocks of the Archipelago, with a maximum radiometric age of 6 Ma (Sibrant *et al*. 2015a; Ramalho *et al*. 2017). Owing to slow gradual subsidence of aging oceanic crust (and volcanic loading in the case of the younger islands), one would expect the islands to subside (Sclater *et al*. 1971) which is true for most islands on the plateau. However, Santa Maria experienced recent significant uplift that started 3.5 Ma ago and which is most likely not related to flexural loading or erosion. Instead, magmatic intrusions/underplating below the oceanic crust is a more probable cause for the uplift (Ramalho *et al*. 2017).

Underplating is defined as large igneous intrusions at the base of the crust, which exhibit seismic velocities that are unusually high for the lower crust (e.g. *P*-wave velocities can exceed 7.6 km s^{-1}), but are still slower than the velocities in the mantle (see, e.g. Caress *et al*. 1995). Magmatic underplating seems to be a common but not universal feature of hot-spot volcanism (e.g. Lodge & Helffrich 2006; Leahy *et al*. 2010; Lodge *et al*. 2012; Fontaine *et al*. 2015). It has mostly been found beneath oceanic volcanic structures emplaced in strong and old lithosphere. In contrast to oceanic islands based on old lithosphere, studies of near-ridge hot-spot volcanism suggest crustal thickening without underplating (e.g. Staples *et al*. 1997; Evangelidis *et al*. 2004).

Silveira *et al*. (2010) investigated the Azores using receiver functions (RFs) and estimated a Moho depth of 20–30 km. However, this study focused mainly on mantle structure by using low-passed filtered RFs that significantly reduce the resolution of fine-scale crustal structure. To date, studies of the islands' seismic structure have only been carried out in limited areas and do not cover the whole Azores Archipelago (e.g. Dias *et al*. 2007). In general, crustal thickness estimates beneath the islands have been in the 10–30 km range (e.g. Detrick *et al*. 1995; Escartin *et al*. 2001), which is much thicker than normal oceanic crust of ∼7 km (e.g. Mutter & Mutter 1993). The thick crust might be related to the influence of a plume, to the building of the Azores Plateau, or to tectonic processes related to the plate movements.

The fine-scale crustal structure beneath the Azores Islands is therefore still poorly known, especially on the western side of the MAR. Here, we use data from nine seismic stations located across the Azores Islands to investigate in detail the crustal structure of the region with teleseismic *P*-wave RFs. We investigated *P*-wave RFs for signals associated with the volcanic edifice, the crust–mantle boundary, a potential underplated layer, and the lithosphere–asthenosphere boundary (LAB) beneath the various islands. Our resulting crustal models can provide new constraints on the formation process of the Azores Plateau, and yield general insight into the dynamics of plume-ridge interaction as well as the tectonics of triple junctions. Accordingly, we focus on the general lithospheric structure beneath the Azores Islands and address the following questions: (1) How thick is the volcanic edifice and the underlying crust, and do the estimated thicknesses reflect the age of the plate, the influence of a plume, or that of tectonic processes along the diffuse plate boundary between Eurasia and Nubia (and particularly along the Terceira Ridge)? (2) Is the crustal structure beneath the islands similar on both sides of the MAR? (3) Is magmatic underplating present beneath ocean islands close to a ridge? (4) Can we observe the LAB beneath the islands and is this feature affected by the plume or the tectonics of the Eurasia-Nubia boundary?

Table 1. Three component broad-band seismic stations from the Azores Islands used in this study.

Station	Location	Latitude (deg)	Longitude (deg)	Elevation (m)	Recording period (available data)	Number of events
CMLA	São Miguel	37.764	−25.524	429	Since 03/1996	43
COV2	Corvo	39.677	−31.113	194	05/2001–09/2002	5
PSMA	Santa Maria	36.995	−25.131	123	12/2000–09/2002	9
ROSA	São Jorge	38.721	−28.247	310	Since 03/2008	30
PSPRB	Santa Maria	36.940	−25.040	290	06/2011–07/2012	14
PSJO	Pico	38.422	−28.303	0 (n/a)	12/2000–09/2002	6
PSCM	Terceira	38.701	−27.117	360	12/2000–09/2002	6
CDRO	Faial	38.629	−28.699	195	Since 07/2001 (07/2000–05/2004)	6

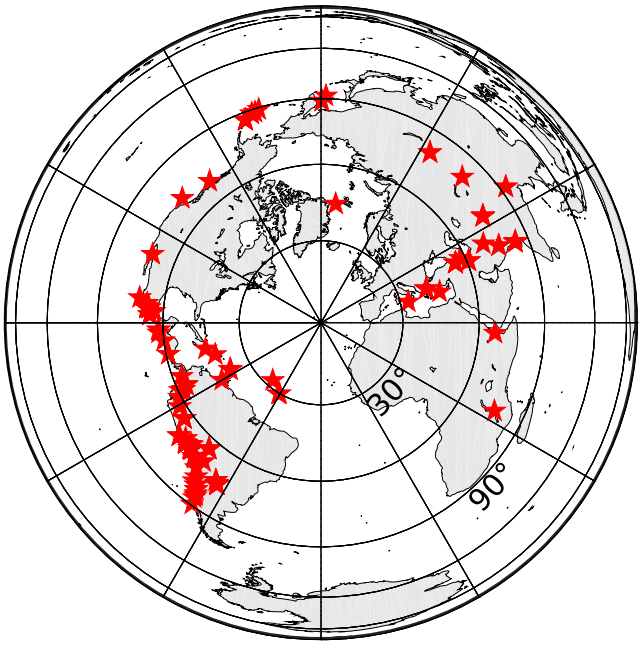

Figure 2. Distribution of earthquakes (red stars) used in this study. The map is centred on the Azores Islands (37.5°N, −28.0°W). The grid indicates the epicentral distances at 30° intervals.

2 DATA

We analysed teleseismic waveforms that were recorded at nine seismic broad-band stations located on the islands of Corvo, Faial, Pico, São Jorge, Terceira, São Miguel and Santa Maria (Fig. 1 and Table 1). Two of these stations are permanent stations CMLA (GSN/IRIS) and ROSA (Portuguese National Seismic Network) deployed in 1996 and 2008, respectively. Moreover, we used recordings from four temporary stations deployed between December 2000 and September 2002 (COV2, PSCM, PSJO, PSMA), and one station (CDRO) that recorded data from 2001 to 2004. An additional three-component broad-band station was deployed from June 2011 to July 2012 on Santa Maria (PSPRB). Two other stations (including one on Flores) were deployed during the same time period but they did not yield sufficient data for processing. As in most standard *P*-wave RF studies (see, e.g. Rondenay *et al*. 2017), we restricted our dataset to high signal-to-noise ratio signals from teleseismic earthquakes of magnitude $M_w \geq 5.5$ that occurred at 30° to 95° epicentral distance from the stations (Fig. 2).

3 METHOD

We employed *P*-wave RF to resolve the crustal structure beneath the Azores Islands. In this section, we describe the various processing steps used to generate and analyse our RFs. These steps include filtering, to reduce the noise and to control the vertical resolution afforded by the signals, and stacking, to further reduce noise and obtain robust RF pulses for interpretation. In terms of analyses, we first used the Hk-stacking method of Zhu & Kanamori (2000), to estimate the number of layers within the crust. We then used forward modelling to obtain a crustal model for the Azores. Both analysis methods rely on direct conversions and reverberations of the crustal layers.

3.1 Receiver function processing

We computed our *P*-wave RFs (e.g. Langston 1979) by rotating the seismic components into the LQT coordinate system (Vinnik 1977) and equalizing the traces using the multi-taper cross-correlation method (Park & Levin 2000; Helffrich 2006; Lekic & Fischer 2014). An advantage of this frequency-domain deconvolution is that frequency-dependent variance weighting can be used when stacking RFs, that is, less weight is given to the portions of the signal most affected by noise (see, e.g. Park & Levin 2016).

After deconvolution, we produced three sets of RFs that highlight different frequency bands of the original deconvolved signal: (i) unfiltered signal—noisy but highest resolution, (ii) bandpass filtered signal with cut-offs at 0.03–1.0 Hz—less noisy and fine scale resolution, and (iii) bandpass filtered signal with cut-offs at 0.03–0.3 Hz—low noise and broad scale resolution. The vertical resolution of the RFs was estimated by taking half of the *S*-wavelength (e.g. Rychert *et al*. 2007) and amounts to ∼1.6 km or ∼5.6 km in the crust using an *S*-wave velocity of 3.36 km s^{-1} (PEM-O; Dziewonski *et al*. 1975) for high cut-offs of 1.0 and 0.3 Hz, respectively. Note, that we based the resolution estimates on the velocity model PEM-O because it is the model that best resembles the average crustal and mantle structure beneath oceans.

The next processing step was stacking of the RFs, which enhances the signal amplitude and reduces the noise. We stacked all RFs obtained at individual stations to obtain a general overview of the crustal structure beneath the stations. However, the travel times of converted phases and their multiples can be affected by short-scale lateral variations in crustal structure, which results in an incoherent sum when the RFs are stacked over the whole epicentral distance range. Therefore, we also generated stacks of RFs that are binned in epicentral distance ranges of 15° (substacks). For each station, we obtained several RF substacks, which we used to estimate the robustness of the pulses contained in the signal. If a pulse was present in all or most of the substacks, it was deemed to be a more robust feature than a pulse that was only present in one substack.

Similar to these epicentral distance substacks, we stacked RFs in backazimuthal bins with a size of 15° and an overlap of 5°, an example can be seen in Supporting Information Fig. S6 for the station CMLA, which has the most RFs and in general a good

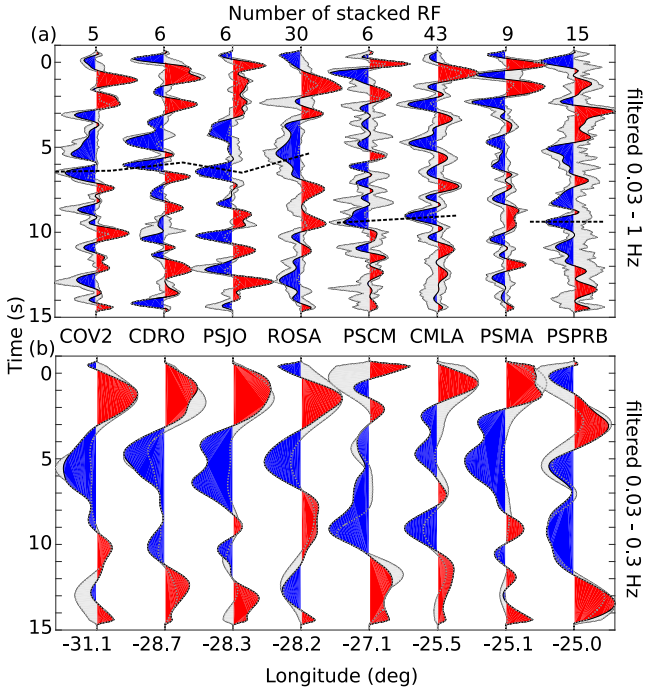

Figure 3. Stacked *P* receiver functions at the Azores seismic stations, filtered with bandpass filters of (a) 0.03 to 1 Hz and (b) 0.03 to 0.3 Hz. The dashed grey lines and grey shaded area indicate the interquartile range as a measure of the spread for all the RFs contributing to a given stack. The receiver functions are sorted by longitude from West to East. The dashed lines in panel (a) mark the signals interpreted to be from the LAB.

backazimuthal coverage. The backazimuthal substacks were created to assess whether events from different directions sample very different structures, something that can happen in a highly heterogeneous ocean island environment. Unfortunately, the backazimuthal coverage is limited for most stations (see Supporting Information Fig. S1) such that often there were not enough RFs within a 15° backazimuthal range for stacking. For some stations, even backazimuthal bin widths of over 30° were not enough to produce substacks. Therefore, we were not able to include a meaningful analysis of possible backazimuthal heterogeneity beneath nearly all of the Azores Islands.

The variability of the individual traces used in the stacks and substacks is expressed via the interquartile range (dashed grey lines and grey shaded area, Fig. 3). In some cases, the two lines marking the interquartile range are not far apart showing that the spread is small. Moreover, the stacks can lie close to the outer range of the interquartile range. Both these observations are more common in the stacks where a long-periodic filter was used.

3.2 Hk-stacking

The first analysis applied to the pre-processed data was the Hk-stacking method of Zhu & Kanamori (2000), which is generally used to estimate the average crustal thickness and the Vp/Vs-ratio. Here we employed it to estimate the number of layers and the depth of interfaces within a multi-layer crust, as has been done in previous RF studies of ocean islands (e.g. Leahy & Park 2005; Leahy *et al*. 2010). An example of this application to a synthetic dataset is presented in the supplementary material (Supporting Information Fig. S2). In our application to real data from the Azores, we assumed an average *P*-wave velocity of Vp = 4.8 km s^{-1} beneath all stations—a value based on global velocity estimates for the volcanic edifice (Mutter & Mutter 1993).

It should be noted, however, that the results of the Hk-stacking method are affected by the chosen input *P*-velocity and by the complexity of crustal structure. Wölbern & Rümpker (2017) showed that the method can produce ambiguous results and that, in general, the resulting Vp/Vs ratios are less reliable than the depths estimates. It has been further demonstrated that departures from an assumed 1-D horizontally layered model can yield flawed Hk-stacking result (Julià 2007; Lombardi *et al*. 2008). Ocean islands pose additional problems: reverberations of converted phases beneath an island might be reflected at the seafloor surrounding the island. This produces multiples that have a shorter travel path than expected and thus arrive earlier than accounted for in the Hk-stacking (e.g. Leahy *et al*. 2010). In light of these limitations, we use the Hk-stacking results only as an initial estimate of the possible conversion depths. Due to the limited recording period of most stations, the backazimuthal coverage was not sufficient to investigate any dipping and/or anisotropic effects in the conversions (Supporting Information Fig. S1; *cf.* Jones & Phinney 1998; Savage 1998). Therefore, our interpretations were restricted to the assumption of horizontal, isotropic layers (Supporting Information Fig. S3).

3.3 Receiver function modelling

The second approach we used was forward modelling to estimate the seismic velocity structure beneath the stations and obtain a crustal model for the Azores Islands. Synthetic RFs were calculated for a range of possible models using the RAYSUM code (Frederiksen & Bostock 2000) and were qualitatively compared with the observed RFs. Due to the lack of backazimuthal coverage, we choose to keep the number of free parameters at a minimum by limiting our modelling to horizontal layers that are laterally continuous. We also limited this comparison to stations that afford sufficient event coverage to produce robust RF stacks. As we will see below, these conditions are met for the two permanent stations, CMLA and ROSA, which have operated for the longest time period (Table 1).

The 1-D velocity models used in the forward modelling can be found in Supporting Information Table S1 and are based on different published velocity models relevant to the Azores: PEM-O, a reference model beneath oceans (Dziewonski *et al*. 1975) that we complemented with a 5 km-thick volcanic edifice layer at the surface (M1); the Crust1.0 model beneath CMLA and ROSA (Laske *et al*. 2013), also complemented with a volcanic layer (M3a,b); and a three-layer ocean island model with or without magmatic underplating based on RF results from Hawaii (Leahy *et al*. 2010; M2a), where M2b and M2c are variations of M2a without underplating. The velocity models M4 to M10 are based on the first three models and the Hk-stacking results (Supporting Information Table S2), and are built to fit the pulses observed in the stacked RF by forward modelling. To steer clear of implausible models, we used estimates from active seismic and gravity studies as guidelines for the layer depths (crustal layer at roughly 3 km), velocities (∼7.6 km s^{-1} at about >12 km) and densities (∼2850 g cm^{-3} in the crust) (Steinmetz *et al*. 1977; Montesinos *et al*. 2003; Nunes *et al*. 2006; Dias *et al*. 2007). In general, the models can be divided into two classes, those with magmatic intrusions beneath the oceanic crust (underplated layer) (M2a, M6, M7a–c, M10) and those with a simple oceanic crust (M1, M2b,c, M3a,b, M4, M5, M8, M9). All models contain an upper crustal layer corresponding to a volcanic edifice of 1–5 km thickness.

Our modelling strategy consisted of building up models first for crustal structure and then expanding into the mantle. We started by matching pulses in the 0–4 s range with crustal interfaces and a Moho. We then investigated whether the addition of a LAB (5 per cent Vs drop) in the 40–90 km depth range, as has been suggested by Silveira *et al.* (2010), is required to reproduce the RF signal between 4 and 10 s.

4 RESULTS

We calculated individual RFs at each station for signals from all events within the prescribed magnitude/epicentral distance ranges (*cf.* Section 2) and retained those which exhibit a stable behaviour (i.e. low 'ringyness' and limited acausal signal; see Supporting Information Fig. S4 for example). This process led to a variable number of usable RFs at each station (Table 1). The first analysis step consisted of investigating RF stacks and substacks with a focus on the arrival times of prominent phases, as these will serve as a basis for the subsequent forward modelling. Our identification of robust phases was aided by results from the Hk-stacking method (*cf.* Supporting Information Table S2). We then concentrated our modelling efforts on finding the crustal/upper mantle structure that best matched the data from the two permanent stations, CMLA and ROSA. Lastly, our preferred models for the permanent stations were used to qualitatively assess the structure below stations that have more limited coverage.

4.1 Robust signals

We started by analysing stacked RFs and focused our attention on peaks that could be identified robustly across all epicentral distance substacks. The full RF stacks for each station are shown in Fig. 3, for two distinct frequency bands. The substack sections, computed with epicentral distance bins that are on average 15° wide and overlap by 5°, are shown in Fig. 4 and Supporting Information Fig. S5. An example of substacks using backazimuthal binning are shown in Supporting Information Fig. S6. Upon initial inspection, we found that the most prominent phases arrive within the first 5 s of the RFs, which suggests a thin-layer structure beneath the islands. Most stacked traces show prominent signals at approximately 0.5, 1 and ∼2.5 to 3 s delay time relative to the *P*-phase (Figs 3 and 4), with the first two signals sometimes joined into a wider pulse. Positive signals indicate an increase in velocity with depth (e.g. the Moho or an underplated layer), whereas negative signals indicate a decrease in velocity. Using background velocities based on the PEM-O model (Dziewonski *et al.* 1975) with the first 5 km modified to fit ocean island velocities, we can convert delay times of 0.5, 1 and 2.5 s into conversion depths of approximately 3, 7, and 18 km, respectively. The Hk-stacking yields similar results with a maximum conversion depth at 13–17 km and a shallow interface at 1–3.5 km depth beneath most islands (Supporting Information Figs S7 and S8, Table S2). These results also suggest the existence of at least one more interface in the 5–13 km depth range beneath the different islands. Departures from a predominantly two to three-layer structure are observed at station PSPRB, with no phases before 1 s and a strong negative arrival at 3 s delay time. Despite PSPRB and PSMA being located on the same island, their stacked RFs differ from one another, especially in the first 1–2 s delay time.

We now consider prominent RF pulses that arrive after 5 s delay time. Based on our modified PEM-O velocity model, such pulses with arrival times of >5 s correspond either to conversions at uppermost mantle depths (>50 km) or to multiples from crustal interfaces. The stations can be subdivided into three classes based on their RF response at delay time >5 s (see Figs 3 and 4): (i) those closest to the MAR (COV2, CDRO, PSJO, ROSA) exhibit a prominent negative phase arriving at 5 to 6.5 s delay time; (ii) those located on the Terceira Ridge (PSCM, CMLA) exhibit a prominent negative phase at ∼9 s delay time; and lastly (iii) those located to the east on the island Santa Maria (PSMA, PSPRB) exhibit smaller but relatively coherent pairs of negative phases that arrive at 5–6

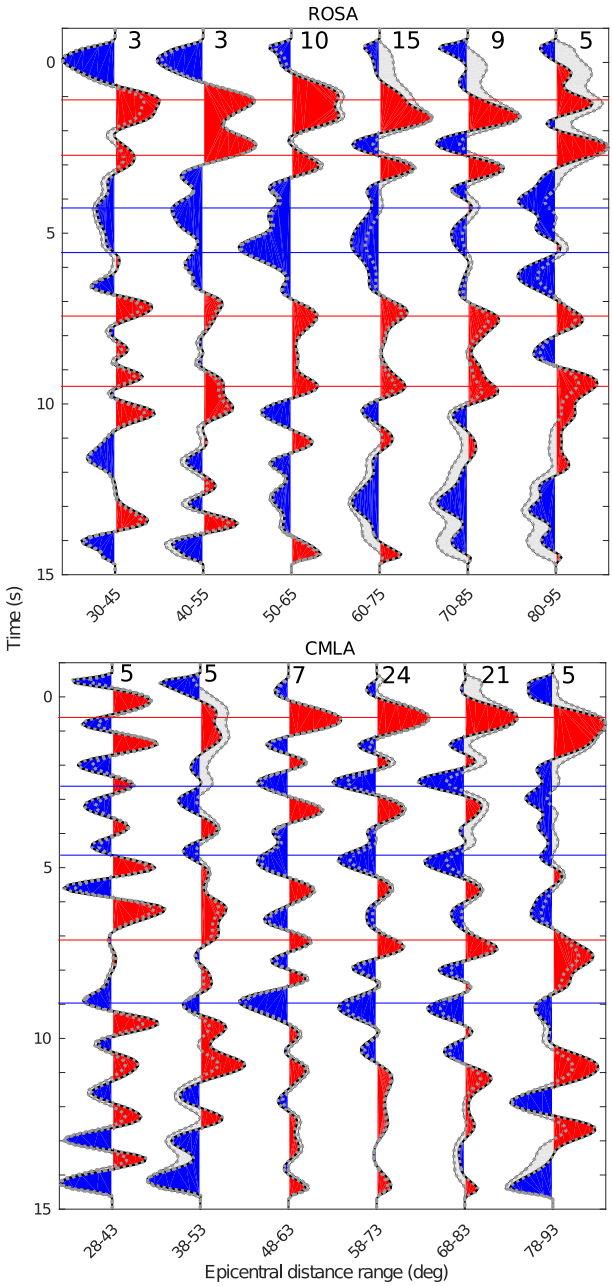

Figure 4. *P* receiver functions at the Azores seismic stations with the most data, stacked in epicentral bins with an average size of 15° and with an overlap of 5 per cent, and filtered with a bandpass filter with cut-offs at 0.03–1.00 Hz (the numbers of RFs in each stack in indicated above each trace, to the left). See also Supporting Information Fig. S5 for epicentral stacks of the other stations. The grey dashed lines and the grey shaded area indicate the interquartile range for each stack. The red and blue lines on CMLA and ROSA sections show the phases modelled in the synthetics.

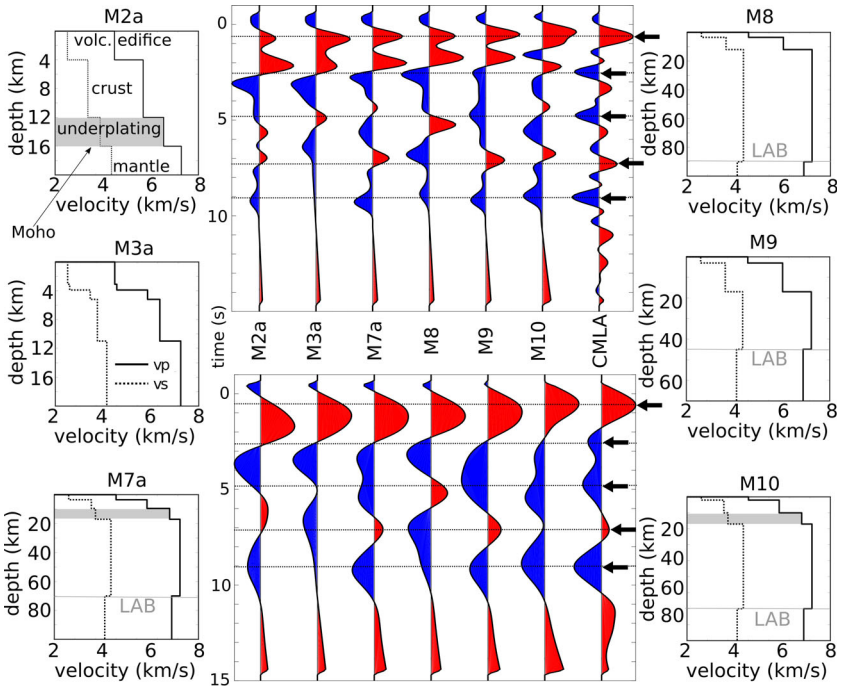

Figure 5. Comparison of stacked receiver function at station CMLA with six stacked synthetic receiver functions. In the upper section, the RFs are bandpass filtered between 0.03 and 1.00 Hz, whereas in the lower section they are bandbass filtered between 0.03 and 0.30 Hz. The synthetic RFs are calculated based on the distribution of earthquakes recorded at CMLA and they are processed in the same manner as the real data. The grey colour band shows the models containing an underplated layer. M2a is based on the velocities derived by Leahy *et al*. (2010) with an underplated layer; layer depths are inferred from literature (Searle 1976; Detrick *et al*. 1995; Luis & Neves 2006; Nunes *et al*. 2006; Dias *et al*. 2007). M3a is based on the Crust 1.0 velocity model at the location of CMLA (Laske *et al*. 2013). M7a includes an underplated layer from ∼10 to 17 km depth, and a 5 per cent reduction of velocities at a depth of 70 km (representing a potential LAB). M8 has a standard two-layer crust extending to 12 km depth and a velocity reduction at a depth of 90 km. M9 has a standard two-layer crust extending to 17 km depth and a velocity reduction at a depth of 45 km. M10 is our preferred model, with an underplated layer from 10 to 17 km and a velocity reduction in the mantle at 70 km depth. The arrows and dashed lines show the phases modelled in the synthetics.

and 8–9 s delay times. If they represent two primary conversions, the signals at 5 to 6 s would correspond to conversion depths of ∼45 to 55 km, whereas those at 9 s would denote a conversion depth of ∼85 km. The source of these signals will be better constrained with the aid of synthetic models.

4.2 Velocity models

The next stage of the analysis aimed to find the velocity models that can best reproduce converted signals observed in the RF stacks of stations CMLA and ROSA. To do so, we compared qualitatively the synthetic RFs from a range of velocity models (Supporting Information Table S1, see also Section 3) to the RFs from these stations, with a focus on the most robust signals (blue and red lines in Fig. 4). Since the main converted phases arrive within a few seconds delay time, we improved the characterization of the results by modelling the multiples that arrive after the main conversions. The main modelling results are shown in the Figs 5 and 6, and additional model outputs and data comparisons are included in the Supporting Information (Figs S9 and S10).

We first considered the forward modelling results for station CMLA. Fig. 5 shows the comparison of synthetic data to the stacked RFs at that station. We have found that the presence of at least two crustal layers, including a thin (∼1–4 km) superficial layer, is necessary to produce the wide positive pulse at 0.8 s and the sequence of positive/negative pulses in the 2.5–9 s time range (compare M2a, M3, M7a versus M8, M9, M10). The addition of a lower crustal, high-velocity layer further helps fine-tune the match to the observed multiples. With this, we found that models M9 and M10 are those which best reproduce the amplitude and arrival time of the conversions and reverberations that were highlighted in Fig. 5. However, most models (including M9) produce an extraneous positive signal in the ∼2–3 s range resulting in a double peak that is not observed in the data. This lack of a double peak in the CMLA stack may be due to the existence of dipping or laterally discontinuous layers that are not accounted for in our models, which only assume horizontally stratification. Such dipping/discontinuous layers would affect the arrival time of the pulses arriving within the first few seconds of the RFs, potentially causing double peaks with variable offsets to interfere and coalesce into a single peak around 0.8 s in the stack. Considering the results of the epicentral distance and backazimuthal stacks of CMLA (Supporting Information Figs S4 and S6), which show evidence of double peaks in the 0.0–2.9 s range within some of the bins, we believe that the models M9 and M10 describe well the structure beneath the station. Model M9 has a normal crustal structure with a LAB at 45 km depth, while M10 includes an additional lower crustal layer with high seismic wave velocities (Vp = 7.6 km s^{-1}, Vs = 4.0 km s^{-1}) and a LAB at 70 km depth. Velocity models that do not include a velocity reduction in the uppermost mantle (i.e. a LAB) fail to adequately reproduce the amplitude and arrival time of phases arriving after 5 s delay time.

For station ROSA we tried to model amplitude and arrival time of the phases marked in Fig. 4 with the various models shown in Fig. 6 (see also Supporting Information Fig. S9). We focused especially on reproducing the prominent positive double peak visible at between

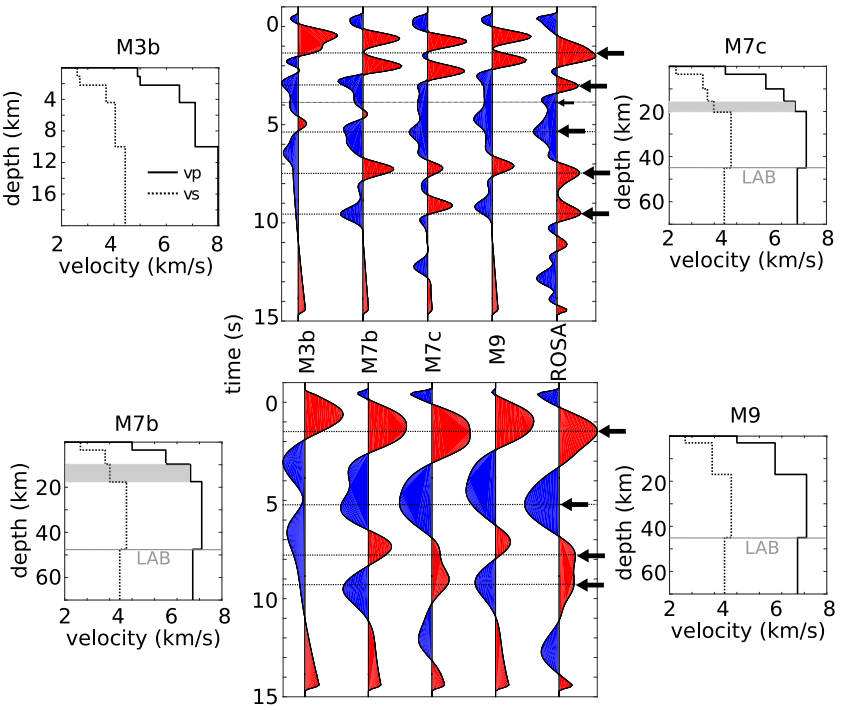

Figure 6. Comparison of stacked receiver function at station ROSA with four stacked synthetic receiver functions. In the upper section, the RFs are bandpass filtered between 0.03 and 1.00 Hz, whereas in the lower section they are bandbass filtered between 0.03 and 0.30 Hz. The synthetic RFs are calculated based on the distribution of earthquakes recorded at ROSA and they are processed in the same manner as the real data. The velocity model M3b is based on the Crust1.0 velocity model at the location of ROSA (Laske *et al*. 2013). The velocity model M7b includes an underplated layer and a 5 per cent velocity reduction at a depth of 48 km (representing a potential LAB). Our preferred model, M7c, has an additional lower crustal layer and a velocity reduction in 50 km. M9 has standard two-layer crust extending to 17 km depth and a velocity reduction in 45 km depth. The grey colour band shows the models containing an underplated layer. The arrows and dashed lines show the phases modelled in the synthetics.

7 and 10 s. Due to its delay time >5 s, the double peak is most probably related to reverberations of two crustal layer boundaries that are close in depth. These multiples were best matched by the output of velocity model M7c (Supporting Information Table S1), which comprises four crustal layers including a lower crustal layer with high seismic wave velocities (Vp = 7.6 km s^{-1}, Vs = 4.0 km s^{-1}). However, we note that there is a time offset of ∼1 s between the first two peaks in the synthetic RFs and those in the real RFs. As in the case of the double pulse in CMLA, we believe that this offset is likely due to the limitations of our models, which assume a horizontal stratification and thus do not take into account dipping of laterally variable interfaces (something that one may expect beneath the islands). Considering these limitations of our models we believe that the preferred models describe sufficiently well the structure beneath the station. A similar double peak is visible in the RF stacks of stations COV2, PSJO and PSMA, which may indicate the existence of a similar lower-crustal high-velocity layer beneath these stations. As with station CMLA, the inclusion of a velocity reduction in the mantle at 45 km is necessary adequately to reproduce the amplitude of the negative pulse observed at 5–6 s in the RFs from ROSA (compare models M3b and M7b,c in Supporting Information Fig. S10).

5 DISCUSSION

Combining the results of the RF stacks and the forward modelling, we interpret our RFs based on simple 1-D isotropic models of the crust with two to three layers, as the limited resolution afforded by the signals precludes consideration of more complex models (e.g. anisotropy, dipping layers). The discussion focuses on constraints that our results can place on the thickness of the volcanic edifice and the depth of the Moho beneath each island. We also address the existence of a potential third layer in the lower crust, which could represent mafic underplated material, and variations in LAB depth across the region. Our preferred interpretation for the structure beneath each island, which we shall discuss in more detail below, is summarized in Fig. 7.

5.1 Base of the volcanic edifice

The interface at a depth of around 1–4 km is interpreted as the base of the volcanic edifice (Fig. 7). The island of Corvo (west of the MAR) and the islands of São Jorge and Santa Maria (east of the MAR) show evidence for a slightly thicker volcanic layer than the other islands. The depth to the base of the edifice varies from island to island owing to the difference in elevation between the different seismic station (Table 1) and to the total volume of the volcanic material that makes up each island (i.e. function of volcanic activity and eruption area). The seafloor around the Azores Islands varies from approximately −1300 m in between the central islands (Faial, Pico, São Jorge) to −3000 m close to the eastern islands (São Miguel, Santa Maria; EMODnet, http://portal.emodnet-bathymetry.eu/), establishing a minimum submerged island edifice height—if we ignore any possible island pedestals buried by seafloor sediment. This minimum height and the elevation of the stations (Table 1) indicate that the base of the volcanic edifice beneath the islands is at approximately 1.5 to 3.5 km depth, which is consistent with our RF results. These observations are also consistent with interfaces found by

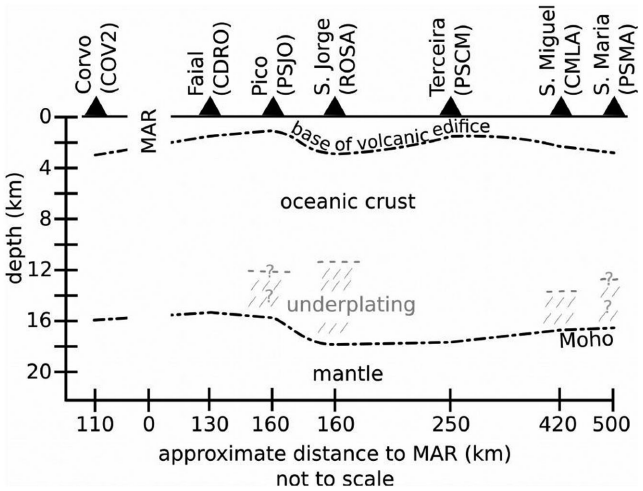

Figure 7. Schematic conversion depths beneath the Azores Islands. The depth is relative to the station elevation (Table 1). The estimated base of the volcanic edifice and the Moho are indicated. The proposed underplated layer is based on the forward modelling results for ROSA and CMLA, as well as the Hk-stacking results (Supporting Information Table S2).

local earthquake tomography at ∼3 km depth beneath the islands of Faial and Pico (e.g. Dias *et al*. 2007), and with the depth to the base of the edifice beneath other volcanic islands such as Hawaii (e.g. Leahy *et al*. 2010).

5.2 Moho

The deeper interface at approximately 17 km depth (∼2.5 s delay time) corresponds most likely to the Moho discontinuity, marking the putative crust–mantle boundary. Subtracting the thickness of the volcanic edifices (1–4 km) from this Moho depth leads to crustal thicknesses in the 13–16 km range for the archipelago. This is a slightly thicker crust than the estimates of 8–12 km from previous studies such as active seismic, gravity, and local earthquake tomography (e.g. Searle 1976; Escartin *et al*. 2001; Luis & Neves 2006; Dias *et al*. 2007). But our Moho depth is in better agreement with these aforementioned studies than with the depth of ∼30 km estimated in a previous RF study (Silveira *et al*. 2010). The difference in the Moho depth between this RF study and that of Silveira *et al*. (2010) can be explained by the low-pass filter used in Silveira *et al*. (2010), which results in a resolution loss for crustal structure. Using such a long-period filter limits the resolution because it produces interference between the separate crustal phases. In the case of the Azores, the phases that may combine include converted signals from the Moho signal, the volcanic edifice, and other crustal layers, as well as multiples. This can result in a broad positive peak that has its maximum shifted to greater depths than the actual Moho depth.

It seems that the crust–mantle boundary is relatively constant beneath all the islands (Fig. 7), indicating that there is low or no correlation between crustal age and Moho depth. However, there is some evidence that the Moho depth is shallowest beneath the islands of the Central Group, especially Faial and Pico (∼15–16 km depth compared to >16 km elsewhere, *cf.* Fig. 7). This might be related to the younger age of the crust compared to the islands further east since evolving crust experiences a slow gradual subsidence (e.g. Sclater *et al*. 1971). It could also be that the younger sites of magmatism in the Central Group islands experienced smaller degrees of crustal thickening by intrusions than elsewhere in the archipelago. The crustal thickness beneath the islands located on the Terceira Ridge (Terceira and São Miguel) is comparable to the crust beneath the other islands. Therefore, it seems that the rift and the tectonic stresses in this region have no significant effect on the crustal thickness. We also cannot find significant differences in Moho depths between the islands located west or east of the MAR.

5.3 Underplating

Magmatic underplating has been found beneath many hot-spot related ocean islands (e.g. Leahy *et al*. 2010; Lodge *et al*. 2012; Fontaine *et al*. 2015), but previous studies of hot-spot related islands in the vicinity of an ocean ridge found no evidence for underplating (e.g. Staples *et al*. 1997; Evangelidis *et al*. 2004). Here, we will show that we can resolve magmatic underplating beneath some of the Azores Islands, which are located close to the Mid-Atlantic ridge.

The RFs at station ROSA show a clear double peak between 7 and 10 s which is best explained by crustal multiples in our forward modelling study (Fig. 6). The results suggest that there are two interfaces in the lower crust, the Moho and an additional, shallower interface. These interfaces form a ∼5 km-thick lower-crustal layer which appears to have seismic velocities of Vp = 7.6 km s^{-1} and Vs = 4.0 km s^{-1} (*cf.* preferred model M7c, Supporting Information Table S2). These velocities appear to lie halfway between values of typical crustal and mantle assemblages, and yield a high Vp/Vs ratio indicative of mafic/ultramafic materials with a possible hydrous alteration component (see, e.g. Christensen 1996). Our preferred value of Vp is in agreement with results from local tomography studies in the vicinity of Faial, which return *P*-wave velocities of approximately 7.6 km s^{-1} for the uppermost mantle just below the crust (Dias *et al*. 2007). Such velocities of 7.6 km s^{-1} are consistent with those usually attributed to magmatic underplating (see, e.g. Watts *et al*. 1985; Caress *et al*. 1995). Thus, along with the location of the layer at the base of the crust, the velocities point to the existence of a zone of magmatic underplating beneath the island of São Jorge. The origin of this inferred underplated layer must lie in the magmatic processes that have affected the island over time. Given the island's proximity to a putative plume, one such process could be that invoked by Jones *et al*. (2015) for the Sierra Leone Rise. In this model, a strongly sheared lithosphere (owing to the triple junction in the Azores case) passing over a mantle plume offers enhanced pathways for melt circulation, leading to accrued melt infiltration and ponding at the base of the crust.

The forward modelling results for the island São Miguel are more ambiguous than those of São Jorge as to whether there is an underplated layer below the oceanic crust or not. When considering broad-spectrum RFs from CMLA (upper section of Fig. 5), we can argue that velocity models that include a high-velocity layer in the lower crust (e.g. M7a, M10) provide a better fit to the positive reverberations at 4 and 7 s delay times than those without such a layer (e.g. M8, M9). We can further designate M10 (underplated layer) as the preferred model as it is the only one that does not produce an extraneous positive peak at ∼2 s. When considering the longer period signals (lower section of Fig. 5), on the other hand, it appears that models M9 (no underplated layer) and M7a (underplated layer) provide the best fits to the positive reverberation at 7 s and the negative one at 9 s. Though model M9 cannot be rejected, the models that contain a high-velocity layer in the lower crust provide good fits in both frequency bands and we can therefore

conclude that an underplated layer is likely present beneath São Miguel.

Due to the very limited data coverage, the RFs of the other islands cannot be used to constrain robustly the existence or the characteristics of an underplated layer beneath them. Nevertheless, there is a trend in the station stacks of Santa Maria (PSMA) and Pico (PSJO) and those of CMLA and ROSA, especially in the first 5 s of the RFs, which could point to underplating beneath these islands as well. Underplating beneath Pico and Santa Maria may be plausible for two reasons: (1) Since the Island Pico is in close proximity to São Jorge, it may be likely that the underplated layer is extending from São Jorge to Pico. (2) The presence of an underplated layer beneath Santa Maria may explain the uplift trend of this island over the last 3.5 Ma years (Ramalho *et al*. 2017). Similar arguments have been made to explain the uplift and evolved volcanism of some of the Canary Islands under which magmatic underplating is seismically observed (Schmincke *et al*. 1997; Klügel *et al*. 2005; Lodge *et al*. 2012). The islands São Miguel and Santa Maria lie on the oldest lithosphere of the Azores Plateau, which could be a factor for accumulation of an underplated layer. Moreover, Santa Maria is the oldest island of the Azores and is located at the southern edge of the 140 km wide shear zone of oblique extensional deformation associated with a diffuse plate boundary, being largely unaffected by active tectonics when compared to the other islands of the Eastern and Central groups (Hipolito *et al*. 2013; Marques *et al*. 2013). Underplating beneath the Canary Islands and Cape Verde shows a loose correlation with age, that is, older islands are more likely to exhibit evidence of underplating (Lodge & Helffrich 2006; Lodge *et al*. 2012).

The existence of an underplated layer at the base of the oceanic crust requires us to reassess what we have defined until now as the Moho. Indeed, our original depth estimate of 17 km for the crust–mantle boundary would in fact correspond to the base of the underplated layer. Based on this, we obtain an estimate of the 'original' oceanic crust beneath the Azores. Let's consider, for example, model M7c, which has a 5 km-thick underplated layer. If we subtract the thickness of the underplated layer and the thickness of the volcanic edifice (1 to 4 km) from our Moho depth estimate, we obtain an original crustal thickness of approximately 8–11 km beneath the underplated islands. This is in very good agreement with previous studies that found 8 to 12 km of crustal thickness in local studies around some islands (e.g. Searle 1976; Escartin *et al*. 2001; Luis & Neves 2006; Dias *et al*. 2007).

5.4 Lithosphere–asthenosphere boundary

A prominent negative phase that is observed in all RFs at delay times of 5–9 s (see Fig. 3b) is best modelled by a velocity decrease with depth occurring 45–85 km beneath the stations. Though we have already formally referred to this structure as the LAB, we can now test the validity of our interpretation by calculating the expected thickness of the lithosphere as a function of age and comparing it to the inferred LAB depth beneath each station. The lithosphere has an average age of ∼10 Ma near the islands of Faial, Pico, São Jorge and Corvo (Azevedo *et al*. 1991; Cannat *et al*. 1999) and ∼45 Ma in the vicinity of Santa Maria (Luis & Miranda 2008). This results in expected LAB depths of approximately 35 and 76 km, respectively, when using the 1300 °C isotherm in the plate cooling models of Stein & Stein (1992). These values are consistent with our observations and thus support our interpretation (see Fig. 3), that is, the depth of the interface is generally shallower beneath the islands closer to the MAR (35–55 km, 5–6.5 s delay time) and deepens with increasing distance to the MAR (∼85 km, ∼9 s delay time). Our results also agree with previous geophysical and geochemical studies which estimated the LAB depth to deepen from ∼35–40 km under the Western and Central Islands to ∼70–80 km under São Miguel and Santa Maria (Gente *et al*. 2003; Silveira *et al*. 2010; Genske *et al*. 2012). There are, however, some ambiguous results at the islands of Terceira and Santa Maria that warrant closer inspection.

Our results suggest that the LAB beneath Terceira has a depth of ∼80 km which is similar to that beneath São Miguel, even though Terceira is closer to the islands showing a LAB depth of ∼40 km. These results would imply that the LAB deepens by up to 40 km over a lateral distance of less than 100 km (distance between São Jorge and Terceira). Such a steep lateral gradient cannot be explained by simple plate cooling models and would thus require localized mantle processes (e.g. small-scale convection) that can alter the thickness of the lithosphere over short scale lengths. One such process could be mantle upwelling associated with a mantle plume centred beneath the islands of Faial, Pico, and São Jorge, as has been proposed by Shorttle *et al*. (2010). A mantle plume rising beneath the Central Islands could erode the lithosphere locally, which could explain a steep gradient in lithospheric thickness. Another possible process could be lithospheric thinning at a spreading centre, but this would produce the opposite of what is seen at Terceira and São Miguel. Both islands are located on the Terceira spreading ridge but show evidence for a thicker lithosphere than beneath and close to the MAR; a thicker lithosphere beneath the Terceira Ridge compared to other spreading ridges was also previously predicted due to the ultra-slow spreading of this ridge that does not result in a thinning of the lithosphere (e.g. Vogt & Jung 2004).

The interpretation of LAB signals beneath Santa Maria is somewhat ambiguous due to the contrasting depth estimates obtained at the two stations that sample the island. Indeed, the long-period stacked RF at stations PSMA and PSPRB suggest LAB depths of ∼45 and 85 km, respectively (see negative signals at 5 and 9 s in Fig. 3b). Though once again there are too few RFs to compare the robustness of these two results, we note that there appears to be a stronger LAB signal in the high-frequency RFs of PSPRB compared to PSMA (see Fig. 3a, and negative pulses at 8–10 s in PSPRB section of Fig. 4). Moreover, considering the age of the lithosphere close to Santa Maria (∼45 Ma) and the lack of recent volcanic eruptions at the surface of the island, it is likely that the LAB depth estimate of ∼85 km obtained at PSPRB is the most realistic of the two. This would give an LAB depth beneath Santa Maria that is comparable to the LAB depth beneath São Miguel and Terceira.

6 CONCLUSIONS

A new set of high-resolution RF results provides us with a clearer view of the lithospheric structure beneath the Azores Islands than was available before. We find that the base of the volcanic edifice is located approximately 1–4 km depth beneath the different islands, in agreement with the edifice height inferred from the bathymetry. The depth of the Moho beneath the Azores islands seems to be fairly constant at approximately 17 km depth, and does not seem to be influenced by plate age, plume location or tectonic environment (i.e. proximity to a ridge or a fracture zone). Furthermore, there is no evidence for differences in crustal structure beneath islands west or east of the MAR. We resolve a ∼5 km thick high-velocity layer in the lower crust beneath São Jorge, which we interpret as magmatic underplating. There is also some evidence (albeit weaker)

for underplating beneath São Miguel. Lastly, we find a LAB at an average depth of ∼40 km beneath the islands Corvo, Faial, Pico and São Jorge, and at an average depth of ∼80 km beneath the islands of Terceira, São Miguel, and Santa Maria. The lithosphere does not seem to be affected by the spreading at the Terceira Ridge and its thickness seems to vary across the archipelago in agreement with a simple plate cooling model.

ACKNOWLEDGEMENTS

This work was supported by the project 'Investigation of Island Uplift of the Azores Island Region' (TH1530/6-1) funded by The German Research Foundation (DFG). SR's contribution to this work was supported by Career Integration Grant 321871-GLImER from the FP7 Marie Curie Actions of the European Commission and by the Research Council of Norway FRINATEK programme through SwaMMIS project 231354. RR acknowledges his IF/01641/2015 contract funded by Fundacao para a Ciencia e a Tecnologia. We also kindly acknowledge the following persons and institutions for their support: our colleagues at the Instituto de Investigação em Vulcanologia e Avaliação de Riscos (IVAR), University of Azores, particularly M.G. Queirós, T. Ferreira, J.L. Gaspar, V. Sousa and E. Sousa; S.P. Ávila, A.C. Rebelo, and C. Melo of CIBIO-Açores; R. Câmara, J. Bairos, N. Moura, and J. Pombo of Serviços de Ambiente da Ilha de Santa Maria; J.M. Freitas at Serviço Florestal das Ilhas das Flores e Corvo; I. Cordeiro at Agência Melo; and SATA Air Azores. We would like to thank Dr Stewart Fishwick, one anonymous reviewer and the editor Dr Ana Ferreira for their valuable comments that greatly improved the manuscript.

REFERENCES

Adam, C., Madureira, P., Miranda, J.M., Lourenço, N., Yoshida, M. & Fitzenz, D., 2013. Mantle dynamics and characteristics of the Azores plateau, *Earth planet. Sci. Lett.,* **362,** 258–271.

Azevedo, J.M.M. & Ferreira, M.P., 2006. The volcanotectonic evolution of Flores Island, Azores (Portugal), *J. Volcanol. Geotherm. Res.,* **156**(1–2), 90–102.

Azevedo, J.M.M., Ferreira, M.P. & Martins, J.A., 1991. The emergent volcanism of Flores Island, Azores (Portugal), *Arquipélago,* **9,** 37–46.

Calvert, A.T., Moore, R.B., McGeehin, J.P. & da Silva, A.M.R., 2006. Volcanic history and $^{40}Ar/^{39}Ar$ and 14C geochronology of Terceira Island, Azores, Portugal, *J. Volcanol. Geotherm. Res.,* **156**(1–2), 103–115.

Cannat, M., Briais, A., Deplus, C., Escartın, J., Georgen, J., Lin, J. & Rabain, A., 1999. Mid-Atlantic Ridge-Azores hotspot interactions: along-axis migration of a hotspot-derived event of enhanced magmatism 10 to 4 Ma ago, *Earth planet. Sci. Lett.,* **173**(3), 257–269.

Caress, D.W., McNutt, M.K., Detrick, R.S. & Mutter, J.C., 1995. Seismic imaging of hotspot-related crustal underplating beneath the Marquesas Islands, *Nature,* **373**(6515), 600–603.

Chovelon, P., 1982. Evolution volcano-tectonique des îles de Faial et Pico, *Thèse, faculté des sciences de la Terre,* Université Paris Sud 11 pp. 242.

Christensen, N.I., 1996. Poisson's ratio and crustal seismology, *J. geophys. Res.,* **101**(B2), 3139–3156.

Detrick, R.S., Needham, H.D. & Renard, V., 1995. Gravity anomalies and crustal thickness variations along the Mid-Atlantic Ridge between 33°N and 40°N, *J. geophys. Res.,* **100**(B3), 3767–3787.

Dias, N.A., Matias, L., Lourenço, N., Madeira, J., Carrilho, F. & Gaspar, J.L., 2007. Crustal seismic velocity structure near Faial and Pico Islands (AZORES), from local earthquake tomography, *Tectonophysics,* **445**(3–4), 301–317.

Dziewonski, A.M., Hales, A.L. & Lapwood, E.R., 1975. Parametrically simple earth models consistent with geophysical data, *Phys. Earth planet. Inter.,* **10**(1), 12–48.

Escartin, J., Cannat, M., Pouliquen, G., Rabain, A. & Lin, J., 2001. Crustal thickness of V-shaped ridges south of the Azores: interaction of the Mid-Atlantic Ridge (36°–39°N) and the Azores hot spot, *J. geophys. Res.,* **106**(B10), 21 719–21 735.

Evangelidis, C.P., Minshull, T.A. & Henstock, T.J., 2004. Three-dimensional crustal structure of Ascension Island from active source seismic tomography, *Geophys. J. Int.,* **159**(1), 311–325.

Fontaine, F.R., Barruol, G., Tkalčić, H., Wölbern, I., Rümpker, G., Bodin, T. & Haugmard, M., 2015. Crustal and uppermost mantle structure variation beneath La Réunion hotspot track, *Geophys. J. Int.,* **203**(1), 107–126.

França, Z.T., Lago, M., Nunes, J.C., Galé, C., Forjaz, V.H., Pueyo, O. & Arranz, E., 2006. Geochemistry of alkaline basalts of Corvo Island (Azores, Portugal): preliminary data, *Geogaceta,* 40, 87–90.

Frederiksen, A.W. & Bostock, M.G., 2000. Modelling teleseismic waves in dipping anisotropic structures, *Geophys. J. Int.,* **141**(2), 401–412.

Genske, F.S., Turner, S.P., Beier, C. & Schaefer, B.F., 2012. The petrology and geochemistry of lavas from the western Azores islands of Flores and Corvo, *J. Petrol.,* **53**(8), 1673–1708.

Genske, F.S., Beier, C., Stracke, A., Turner, S.P., Pearson, N.J., Hauff, F. & Haase, K.M., 2016. Comparing the nature of the western and eastern Azores mantle, *Geochim. Cosmochim. Acta,* **172,** 76–92.

Gente, P., Dyment, J., Maia, M. & Goslin, J., 2003. Interaction between the Mid-Atlantic Ridge and the Azores hot spot during the last 85 Myr: emplacement and rifting of the hot spot-derived plateaus, *Geochem. Geophys. Geosyst.,* **4**(10), doi:10.1029/2003GC000527.

Helffrich, G., 2006. Extended-time multitaper frequency domain cross-correlation receiver-function estimation, *Bull. seism. Soc. Am.,* **96**(1), 344–347.

Hildenbrand, A., Madureira, P., Marques, F.O., Cruz, I., Henry, B. & Silva, P., 2008. Multi-stage evolution of a sub-aerial volcanic ridge over the last 1.3 Myr: S. Jorge Island, Azores Triple Junction, *Earth planet. Sci. Lett.,* **273**(3–4), 289–298.

Hildenbrand, A., Marques, F.O., Costa, A.C.G., Sibrant, A.L.R., Silva, P.F., Henry, B., Miranda, J.M. & Madureira, P., 2012. Reconstructing the architectural evolution of volcanic islands from combined K/Ar, morphologic, tectonic, and magnetic data: the Faial Island example (Azores), *J. Volcanol. Geotherm. Res.,* **241,** 39–48.

Hipolito, A., Madeira, J., Carmo, R. & Gaspar, J.L., 2013. Neotectonics of Graciosa, Island (Azores): a contribution to seismic hazard assessment of a volcanic area in a complex geodynamic setting, *Ann. Geophys.,* **56**(6), doi:10.4401/ag-6222.

Ito, G. & Lin, J., 1995. Oceanic spreading center-hotspot interactions: constraints from along-isochron bathymetric and gravity anomalies, *Geology,* **23**(7), 657–660.

Johnson, C.L., Wijbrans, J.R., Constable, C.G., Gee, J., Staudigel, H., Tauxe, L., Forjaz, V.H. & Salgueiro, M., 1998. $^{40}Ar/^{39}Ar$ ages and paleomagnetism of São Miguel lavas, Azores, *Earth planet. Sci. Lett.,* **160**(3–4), 637–649.

Jones, C.H. & Phinney, R.A., 1998. Seismic structure of the lithosphere from teleseismic converted arrivals observed at small arrays in the southern Sierra Nevada and vicinity, California, *J. geophys. Res.,* **103**(B5), 10 065–10 090.

Jones, E.J.W., McMechan, G.A. & Zeng, X., 2015. Seismic evidence for crustal underplating beneath a large igneous province: the Sierra Leone Rise, equatorial Atlantic, *Mar. Geol.,* **365,** 52–60.

Julià, J., 2007. Constraining velocity and density contrasts across the crust–mantle boundary with receiver function amplitudes, *Geophys. J. Int.,* **171**(1), 286–301.

Klügel, A., Hansteen, T.H. & Galipp, K., 2005. Magma storage and underplating beneath Cumbre Vieja volcano, la Palma (Canary Islands), *Earth planet. Sci. Lett.,* **236**(1), 211–226.

Langston, C.A., 1979. Structure under Mount Rainier, Washington, inferred from teleseismic body waves, *J. geophys. Res.,* **84**(B9), 4749–4762.

Laske, G., Masters, G., Ma, Z. & Pasyanos, M., 2013. Update on CRUST1.0—A 1-degree global model of Earth's crust, in *Geophys. Res. Abstr.,* **15,** 2658.

Leahy, G.M. & Park, J., 2005. Hunting for oceanic island Moho, *Geophys. J. Int.,* **160**(3), 1020–1026.

Leahy, G.M., Collins, J.A., Wolfe, C.J., Laske, G. & Solomon, S.C., 2010. Underplating of the Hawaiian Swell: evidence from teleseismic receiver functions, *Geophys. J. Int.,* **183**(1), 313–329.

Lekić, V. & Fischer, K.M., 2014. Contrasting lithospheric signatures across the western United States revealed by Sp receiver functions, *Earth planet. Sci. Lett.,* **402,** 90–98.

Lodge, A. & Helffrich, G., 2006. Depleted swell root beneath the Cape Verde Islands, *Geology,* **34**(6), 449–452.

Lodge, A., Nippress, S.E.J., Rietbrock, A., García-Yeguas, A. & Ibáñez, J.M., 2012. Evidence for magmatic underplating and partial melt beneath the Canary Islands derived using teleseismic receiver functions, *Phys. Earth planet. Inter.,* **212,** 44–54.

Lombardi, D., Braunmiller, J., Kissling, E. & Giardini, D., 2008. Moho depth and Poisson's ratio in the Western-Central Alps from receiver functions, *Geophys. J. Int.,* **173**(1), 249–264.

Lourenço, N.L.J.F., Miranda, J.M., Luis, J.F., Ribeiro, A., Victor, L.M., Madeira, J. & Needham, H.D., 1998. Morpho-tectonic analysis of the Azores Volcanic Plateau from a new bathymetric compilation of the area, *Mar. Geophys. Res.,* **20**(3), 141–156.

Luis, J.F. & Miranda, J.M., 2008. Reevaluation of magnetic chrons in the North Atlantic between 35°N and 47°N: Implications for the formation of the Azores Triple Junction and associated plateau, *J. geophys. Res.,* **113**(B10), doi:10.1029/2007JB005573.

Luis, J.F. & Neves, M.C., 2006. The isostatic compensation of the Azores Plateau: a 3D admittance and coherence analysis, *J. Volcanol. Geotherm. Res.,* **156**(1–2), 10–22.

Luis, J.F., Miranda, J.M., Galdeano, A., Patriat, P., Rossignol, J.C. & Victor, L.M., 1994. The Azores triple junction evolution since 10 Ma from an aeromagnetic survey of the Mid-Atlantic Ridge, *Earth planet. Sci. Lett.,* **125**(1-4), 439–459.

Madeira, J. & Ribeiro, A., 1990. Geodynamic models for the Azores triple junction: a contribution from tectonics, *Tectonophysics,* **184**(3–4), 405–415.

Marques, F.O., Catalão, J.C., DeMets, C., Costa, A.C.G. & Hildenbrand, A., 2013. GPS and tectonic evidence for a diffuse plate boundary at the Azores Triple Junction, *Earth planet. Sci. Lett.,* **381,** 177–187.

Miranda, J.M., Luis, J.F., Lourenço, N. & Fernandes, R.M.S., 2015. The structure of the Azores triple junction: implications for São Miguel Island, *Geol. Soc., Lon, Mem.,* **44**(1), 5–13.

Montesinos, F.G., Camacho, A.G., Nunes, J.C., Oliveira, C.S. & Vieira, R., 2003. A 3-D gravity model for a volcanic crater in Terceira Island (Azores), *Geophys. J. Int.,* **154**(2), 393–406.

Mutter, C.Z. & Mutter, J.C., 1993. Variations in thickness of layer 3 dominate oceanic crustal structure, *Earth planet. Sci. Lett.,* **117**(1–2), 295–317.

Nunes, J.C., Camacho, A., França, Z., Montesinos, F.G., Alves, M., Vieira, R. & Ortiz, E., 2006. Gravity anomalies and crustal signature of volcano-tectonic structures of Pico Island (Azores), *J. Volcanol. Geotherm. Res.,* **156**(1–2), 55–70.

Park, J. & Levin, V., 2000. Receiver functions from multiple-taper spectral correlation estimates, *Bull. seism. Soc. Am.,* **90**(6), 1507–1520.

Park, J. & Levin, V., 2016. Statistics and frequency-domain moveout for multiple-taper receiver functions, *Geophys. J. Int.,* **207**(1), 512–527.

Ramalho, R.S. *et al.*, 2017. Emergence and evolution of Santa Maria Island (Azores)—The conundrum of uplifted islands revisited, *Bull. geol. Soc. Am.,* **129,** 372–390

Rondenay, S., Spieker, K., Sawade, L., Halpaap, F. & Farestveit, M., 2017. GLImER: A New Global Database of Teleseismic Receiver Functions for Imaging Earth Structure, *Seismol. Res. Lett.,* **88**(1), 39–48.

Rychert, C.A., Rondenay, S. & Fischer, K.M., 2007. *P*-to-*S* and *S*-to-*P* imaging of a sharp lithosphere–asthenosphere boundary beneath eastern North America, *J. geophys. Res.,* **112**(B8), doi:10.1029/2006JB004619.

Savage, M.K., 1998. Lower crustal anisotropy or dipping boundaries? Effects on receiver functions and a case study in New Zealand, *J. geophys. Res.,* **103**(B7), 15 069–15 087.

Schilling, J.G., 1975. Azores mantle blob: rare-earth evidence, *Earth planet. Sci. Lett.,* **25**(2), 103–115.

Schmincke, H.U., Behncke, B., Grasso, M. & Raffi, S., 1997. Evolution of the northwestern Iblean Mountains, Sicily: uplift, Plicocene/Pleistocene sea-level changes, paleoenvironment, and volcanism, *Geol. Rundsch.,* **86**(3), 637–669.

Sclater, J.G., Anderson, R.N. & Bell, M.L., 1971. Elevation of ridges and evolution of the central eastern Pacific, *J. geophys. Res.,* **76**(32), 7888–7915.

Searle, R.C., 1976. Lithospheric structure of the Azores Plateau from Rayleigh-wave dispersion, *Geophys. J. Int.,* **44**(3), 537–546.

Searle, R., 1980. Tectonic pattern of the Azores spreading centre and triple junction, *Earth planet. Sci. Lett.,* **51**(2), 415–434.

Shorttle, O., Maclennan, J. & Jones, S.M., 2010. Control of the symmetry of plume-ridge interaction by spreading ridge geometry, *Geochem. Geophys. Geosyst.,* **11**(7), doi:10.1029/2009GC002986.

Sibrant, A.L.R., Hildenbrand, A., Marques, F.O. & Costa, A.C.G., 2015. Volcano-tectonic evolution of the Santa Maria Island (Azores): implications for paleostress evolution at the western Eurasia-Nubia plate boundary, *J. Volcanol. Geotherm. Res.,* **291,** 49–62.

Sibrant, A.L.R. *et al.*, 2015. Morpho-structural evolution of a volcanic island developed inside an active oceanic rift: S. Miguel Island (Terceira Rift, Azores), *J. Volcanol. Geotherm. Res.,* **301,** 90–106.

Silveira, G., Stutzmann, E., Davaille, A., Montagner, J.P., Mendes-Victor, L. & Sebai, A., 2006. Azores hotspot signature in the upper mantle, *J. Volcanol. Geotherm. Res.,* **156**(1–2), 23–34.

Silveira, G., Vinnik, L., Stutzmann, E., Farra, V., Kiselev, S. & Morais, I., 2010. Stratification of the Earth beneath the Azores from P and S receiver functions, *Earth planet. Sci. Lett.,* **299**(1–2), 91–103.

Staples, R.K., White, R.S., Brandsdóttir, B., Menke, W., Maguire, P.K. & McBride, J.H., 1997. Färoe-Iceland Ridge Experiment 1. Crustal structure of northeastern Iceland, *J. geophys. Res.,* **102**(B4), 7849–7866.

Stein, C.A. & Stein, S., 1992. A model for the global variation in oceanic depth and heat flow with lithospheric age, *Nature,* **359**(6391), 123–129.

Steinmetz, L., Whitmarsh, R.B. & Moreira, V.S., 1977. Upper mantle structure beneath the Mid-Atlantic Ridge north of the Azores based on observations of compressional waves, *Geophys. J. Int.,* **50**(2), 353–380.

Vinnik, L.P., 1977. Detection of waves converted from P to SV in the mantle, *Phys. Earth planet. Inter.,* **15**(1), 39–45.

Vogt, P.R. & Jung, W.Y., 2004. The Terceira Rift as hyper-slow, hotspot-dominated oblique spreading axis: a comparison with other slow-spreading plate boundaries, *Earth planet. Sci. Lett.,* **218**(1–2), 77–90.

Watts, A.B., Ten Brink, U.S., Buhl, P. & Brocher, T.M., 1985. A multichannel seismic study of lithospheric flexure across the Hawaiian–Emperor seamount chain, *Nature,* **315**(6015), 105–111.

Wölbern, I. & Rümpker, G., 2017. Limitations of H-κ stacking: ambiguous results caused by crustal layering, *J. Seismol.,* **21,** 221–235.

Zhu, L. & Kanamori, H., 2000. Moho depth variation in southern California from teleseismic receiver functions, *J. geophys. Res.,* **105**(B2), 2969–2980.

SUPPORTING INFORMATION

Supplementary data are available at *GJI* online.

Figure S1. Hk-stacking result for synthetic data based on velocity model M10, which comprises a three-layer crust (interfaces at 2, 10 and 17 km depths) and an LAB at 70 km depth. The global and two local maxima are indicated with a black star. The global maximum is at 2 km depth and has a Vp/Vs ratio of 1.81. The local maxima are at 8 and 11.5 km depth with Vp/Vs ratios of 1.60 and 1.90, respectively. The global maximum is consistent with the top layer of the input velocity model. The local maxima, on the other hand, deviate by ∼2 and ∼5.5 km in depth with the lower boundaries, which is potentially caused by the fixed *P*-wave input velocity of 4.8 km s^{-1}. Nevertheless, these results suggest that the Hk-stacking can identify the presence of three layers, as has been argued by Leahy *et al*. (2010).

Figure S2. Example of backazimuthal coverage at the two permanent stations CMLA and ROSA, as well as station PSCM located on Terceira.
Figure S3. Tangential *P* receiver functions at station CMLA bandpass filtered between 0.03 and 1 Hz. The individual receiver functions are sorted by backazimuth.
Figure S4. Individual *P* receiver functions at station CMLA, bandpassed filtered between 0.03 and 1.00 Hz. The receiver functions are sorted by epicentral distance.
Figure S5. *P* receiver functions at the Azores seismic stations, stacked in epicentral bins with an average size of 15° and with an overlap of 5 per cent, and filtered with a bandpass filter with cut-offs at 0.03–1.00 Hz (the numbers of RFs in each stack in indicated above each trace, to the left). See also Fig. 4 for epicentral stacks of the other stations. The grey dashed lines and the grey shaded area indicate the interquartile range for each stack.
Figure S6. *P* receiver functions at station CMLA (unfiltered) stacked in backazimuthal bins with a size of 15° and with 5° overlap. The grey dashed lines and the grey shaded area indicate the interquartile range.
Figure S7. Hk-stacking results for station CMLA. The global and the first two local maxima are indicated with black stars. The global maximum is at 5.5 km depth and has a Vp/Vs ratio of 1.7. The other maxima are at 1.5 and 13 km depths with Vp/Vs ratios of 1.96 and 1.69, respectively.
Figure S8. Hk-stacking result for station CDRO. The global and three local maxima are indicated with black stars. The global maximum is at 4.5 km depth and has a Vp/Vs ratio of 1.96. The other maxima are at 1.5, 9.5 and 15.5 km depths with Vp/Vs ratios of 1.97, 1.81 and 1.72, respectively.
Figure S9. Comparison of stacked receiver function at station CMLA with nine stacked synthetic receiver functions. In the upper section, the RFs are bandpass filtered between 0.03 and 1.00 Hz, whereas in the lower section they are bandbass filtered between 0.03 and 0.30 Hz. The synthetic RFs are calculated based on the distribution of earthquakes recorded at CMLA and they are processed in the same manner as the real data. Velocity model M1 is based on PEM-O (Dziewonski *et al*. 1975). M2a and M2b are based on the velocities derived by Leahy *et al*. (2010) with an underplated layer and without underplating, respectively; the layer depths are inferred from the literature (Searle 1976; Detrick *et al*. 1995; Luis & Neves 2006; Nunes *et al*. 2006; Dias *et al*. 2007). M3 is based on the Crust1.0 velocity model at the location of CMLA (Laske *et al*. 2013). M4 uses the same velocities as M2a but the interface depths are inferred from Hk-stacking. M5, M6 and M7a are velocity models that are built around a basic three-layer crustal model (M6) that includes an underplated layer between ∼9.5 and 17 km depth. M5 comprises an additional thin sediment layer (0.1 km) at the top, and M7a has a 5 per cent reduction of velocities at a depth of 70 km that represents the LAB (grey line) beneath CMLA. An underplated layer is marked with a grey band in the velocity-depth diagrams.
Figure S10. Comparison of stacked receiver function at station ROSA with two stacked synthetic receiver functions; In the upper section, the RFs are bandpass filtered between 0.03 and 1.00 Hz, whereas in the lower section they are bandbass filtered between 0.03 and 0.30 Hz. The synthetic RFs are calculated based on the distribution of earthquakes recorded at ROSA and they are processed in the same manner as the real data. Velocity model M2b, which does not include underplating, is the same as in Fig. 5. M2c resembles M2b but includes a 5 per cent reduction of velocities at a depth of 50 km that represents the LAB beneath ROSA (grey line). Model M3b is based on the Crust1.0 velocity model at the location of ROSA (Laske *et al*. 2013). Model M7b includes an underplated layer (grey band) and a 5 per cent reduction of velocities at a depth of 48 km. M7c has an additional layer in the lower crust and a velocity reduction (LAB) at 50 km depth.
Table S1. Velocity models used for synthetic modelling. The models M1 to M3 are based on the PEM-O velocity model (Dziewonski *et al*. 1975), the velocity model in Leahy *et al*. (2010) and Crust1.0 (Laske *et al*. 2013), respectively. The velocity models M4 to M10 are based on the first three models and the Hk-stacking results to fit the pulses in the stacked RF by forward modelling. To not use models with implausible data, we used estimates from active seismic and gravity studies as guidelines for the layer depths (crustal layer at roughly 3 km), velocities (∼7.6 km s^{-1} at about >12 km) and densities (∼2850 g cm^{-3} in the crust) (Steinmetz *et al*. 1977; Montesinos *et al*. 2003; Nunes *et al*. 2006; Dias *et al*. 2007).
Table S2. Results of the Hk-stacking.

Please note: Oxford University Press is not responsible for the content or functionality of any supporting materials supplied by the authors. Any queries (other than missing material) should be directed to the corresponding author for the paper.